minerals

MDPI

Article

Effect of Quartz on the Preparation of Sodium Stannate from Cassiterite Concentrates by Soda Roasting Process

Yuanbo Zhang, Benlai Han, Zijian Su *, Xijun Chen, Manman Lu, Shuo Liu, Jicheng Liu and Tao Jiang

School of Minerals Processing and Bioengineering, Central South University, Changsha 410083, China; zybcsu@126.com (Y.Z.); hblcsu@126.com (B.H.); 17786528627@163.com (X.C.); lmmcsu@163.com (M.L.); lsus91@163.com (S.L.); ljccsu@126.com (J.L.); jiangtao@csu.edu.cn (T.J.)

* Correspondence: suzijian@csu.edu.cn; Tel.: (+86)-731-88877214

Received: 19 August 2019; Accepted: 25 September 2019; Published: 1 October 2019

Abstract: Sodium stannate (Na_2SnO_3) has been successfully prepared by a novel process of roasting cassiterite concentrates and sodium carbonate (Na_2CO_3) under CO–CO_2 atmosphere, namely soda roasting-leaching process. However, more than 22 wt. % tin of the cassiterite was not converted into Na_2SnO_3 and entered the leach residues. Quartz (SiO_2) is the predominant gangue in the cassiterite, and phase evolution of SnO_2–SiO_2–Na_2CO_3 system roasted under CO–CO_2 atmosphere was still uncertain. In this study, the effect of SiO_2 in cassiterite concentrates on preparation of Na_2SnO_3 was clarified. The results indicated that $Na_8SnSi_6O_{18}$ was inevitably formed when cassiterite and Na_2CO_3 were roasted above 775 °C under CO–CO_2 atmosphere via the reaction of $SnO_2 + 6SiO_2 + 4Na_2CO_3 = Na_8SnSi_6O_{18} + 4CO_2$, and formation of $Na_8SnSi_6O_{18}$ would be increased with increasing roasting temperature and Si/Sn mole fraction. In addition, it was found that $Na_8SnSi_6O_{18}$ was insoluble in the leachate at pH value range of 1–14, which, therefore, was enriched in the leach residues. The silicon content of the cassiterite concentrates should be controlled as lower as possible to obtain a higher conversion ratio of Na_2SnO_3.

Keywords: sodium stannate; cassiterite concentrates; silicon oxide; sodium stannic silicate

1. Introduction

Sodium stannate (Na_2SnO_3) is highly desirable in many fields, including electroplating [1], tin alloy production [2], and solid superbase catalysts for dehydrogenation and flame retardants [3,4]. Recently, it is also used as solid electrolytes and electrode materials in chemical sources of electrical energy [5]. The consumption of sodium stannate has been increasing rapidly in the last decade. The traditional Na_2SnO_3 preparation processes applied metallic tin and low-melting-point sodium hydroxide (NaOH) as raw materials, which were conducted in a fused state in the presence of sodium nitrate ($NaNO_3$) as oxidizers [6]. However, metallic tin was always obtained from high-temperature reduction smelting process. Besides, some secondary tin-containing resources, including stanniferous alloy, tin scrap, waste solder, and electronic waste, have also been used for preparing sodium stannate [7–13], and these processes would cause high production cost and long process flow. In addition, the emission of hazardous gases (NH_3 and NO*x*) deriving from the oxidizers ($NaNO_3$) was also a shortcoming.

The authors' group has developed a novel process for preparing Na_2SnO_3 from cassiterite concentrates (SnO_2) and sodium carbonate (Na_2CO_3) roasted in a solid-state under CO–CO_2 atmosphere [14,15], namely soda roasting–leaching process. Sodium stannate trihydrate ($Na_2SnO_3{\cdot}3H_2O$) with a purity of 95.8 wt. % was obtained, which met the requirement of industrial first-grade products.

This process displays a bright prospect in preparing Na_2SnO_3, and the function mechanism and the formation kinetics of Na_2SnO_3 have also been clarified in previous publications [16–19]. It was found that CO–CO_2 atmosphere promoted the formation of oxygen deficiency on the surface of cassiterite, which broke the stable structure of SnO_2. Then the activation energy of the reactions between Na_2CO_3 and SnO_2 decreased significantly, and the formation of Na_2SnO_3 was much easily under CO–CO_2 atmosphere [15–20]. Nevertheless, it was found that over 22 wt. % tin of the cassiterite was not converted into Na_2SnO_3 and disposed as residues during the roasting–leaching process [20].

Quartz (SiO_2) is the predominant gangue mineral in cassiterite ores, which cannot be separated perfectly by beneficiation combined methods, such as gravity concentration and froth flotation [21,22]. Before used as raw materials, the cassiterite concentrates should be firstly pretreated by oxidation roasting–acid leaching process to remove the impurity elements, including Fe, As, S, Pb, Sb, etc. [23,24]. However, the quartz (SiO_2) is very hard to be removed during the pretreatment process.

Our previous studies have discussed in detail about the formation mechanism of Na_2SnO_3; however, the reaction principle and thermodynamic data of Na_2CO_3–SnO_2–SiO_2 system were unclear [25–27]. Hence, the major objectives of this study were: (1) to determine the effect of SiO_2 on the leaching efficiency of Sn and Si; (2) to investigate the effect of SiO_2 on phase evolution of SnO_2–Na_2CO_3 system; (3) to ascertain leaching characteristics of the tin, silicon-containing compounds.

2. Materials and Methods

2.1. Materials

As described in our previous studies [14], firstly, cassiterite concentrates were roasted in air at 900 °C for 120 min and then leached with 25% HCl to remove the main impurity elements, including Fe, As, S, Pb, and Sb. The chemical compositions of the original and pretreated cassiterite concentrates are given in Table 1. All the testing samples were pre-ground to a particle size passing through a 200 mesh screen (<0.074 mm). The gases used in this study included CO, CO_2, and N_2 gases, all of which were with purity of 99.99 vol. %.

Table 1. Chemical compositions of the original and retreated cassiterite concentrates (wt. %).

Element	Sn	Si	Fe	CaO	S	Al_2O_3	Zn	As	Pb
Raw material	42.9	3.9	8.86	8.31	5.11	1.16	1.21	0.50	0.38
Pretreated	62.9	3.7	0.11	0.17	0.04	0.28	0.02	0.03	0.03

Analytically pure Na_2CO_3, SnO_2, and SiO_2 were also used to investigate the reaction mechanism.

2.2. Methods

2.2.1. Roasting Process

Sodium salt roasting was one of the effective methods to treat minerals [28–31]. The roasting tests were performed in the high-temperature zone of a horizontal electric resistance furnace. An experimental schematic diagram for the roasting tests is the same as that reported in the previous study [16,32]. The materials were weighed precisely at a certain molar ratio and mixed up gently with an agate mortar and pestle for 30 min. After that, mixed samples were dried in a drying oven at 105 °C for 4 h and then a dried sample about 5.0 g was placed in a corundum crucible (80 mm × 10 mm) and loaded into a heat resistant corundum tube (diameter 45 mm). The crucible carrying the sample was pushed toward the constant roasting zone located in the central area of an electrically heated horizontal tube furnace. Beforehand, N_2 gas was introduced into the corundum tube until the temperature reached a constant value. Next, the N_2 was immediately replaced by the mixed CO–CO_2 gas. Inlet gas flow rate was fixed at 4.0 L/min. The sample was then roasted in a 15 vol. % CO atmosphere at a given temperature (775 °C, 825° C, 875 °C, and 925 °C) for different roasting time (5 min, 10 min, 15 min,

20 min, 30 min, and 60 min). After that, the roasted samples were cooled in pure N_2 atmosphere. Finally, the cooled samples were ready for further analyses.

2.2.2. Leaching Process

The leaching tests were conducted in 250 mL round bottom flasks with a mechanical stirring paddle, and the stirring rate was fixed at 300 rpm for each test. A water bath was used to control the temperature at 40 °C. Next, the ground roasted products of 10.0 g and distilled water of 40 mL were put into the flasks and leached at a fixed pH solution for 60 min in the water bath (pH was fixed at 12.5 based on our previous study [14]). Finally, the leaching solution was filtered and prepared for the determination of Sn and Si concentration. The residues were washed with distilled water to identify the phase constituents.

The leaching efficiency of Sn and Si, which is calculated according to the following equation:

$$L = \frac{1000CV}{MW}100\% \quad (1)$$

where L is the leaching efficiency of Sn or Si, M is the weight of the roasted samples (g), W is the Sn or Si grade of the roasted samples (%), C is the mass concentration of Sn or Si in the leaching solution (mg/mL), and V is the volume of leaching solution (mL).

2.2.3. Instrument Techniques

The chemical compositions of cassiterite concentrates were examined using an X-ray fluorescence spectrometer (XRF, Axios MAX, PANalytical, Almelo, The Netherlands). The phase constituents of the samples were identified by X-ray diffraction (XRD; D/max 2550PC, Rigaku Co. Ltd, Tokyo, Japan) with the step of 0.02° at $10°\cdot min^{-1}$ ranging from 10° to 80°. The content of Sn and Si in the solid material and the aqueous solution were determined using inductively coupled plasma atomic emission spectroscopy (ICP-AES; Icap7400 Radial, Thermo Fisher Scientific, Waltham, MA, USA).

3. Results and Discussion

3.1. Behaviour of Si during the Soda Roasting-Leaching Processs

3.1.1. Effect of Roasting Temperatures and Time

Our previous studies showed that trihydrate sodium stannate ($Na_2SnO_3\cdot 3H_2O$) was obtained by roasting cassiterite concentrates and Na_2CO_3 in CO–CO_2 atmosphere [14], and other impurity elements were almost removed in the pretreatment process. However, the pretreated cassiterite concentrates still contained 3.66 wt. % Si. To examine the impact of SiO_2 on the formation of Na_2SnO_3, the leaching efficiency of Sn and Si was firstly investigated at different roasting temperatures and time.

Figures 1 and 2 illustrate the effect of roasting temperatures and roasting time on leaching efficiency of Sn and Si under the setting experimental conditions: CO content of 15% and Na_2CO_3/SnO_2 mole ratio of 1.5.

It was observed from Figure 1 that the roasting temperatures had significant impact on leaching efficiency of Sn and Si. The leaching efficiency of Sn and Si increased with increasing the roasting temperatures. The leaching efficiency of Sn and Si increased significantly as roasting temperatures increased from 800 °C to 1000 °C. At 1000 °C, the leaching efficiency of Sn and Si was almost the same level, 97.5 wt. % and 96.1 wt. %, respectively. The melting point of Na_2CO_3 is reported as 851 °C, and melted Na_2CO_3 is inclined to volatilize, which resulted in equipment corrosion at higher temperatures [33,34]. Therefore, 875 °C is selected to be a suitable roasting temperature based on the previous study [14].

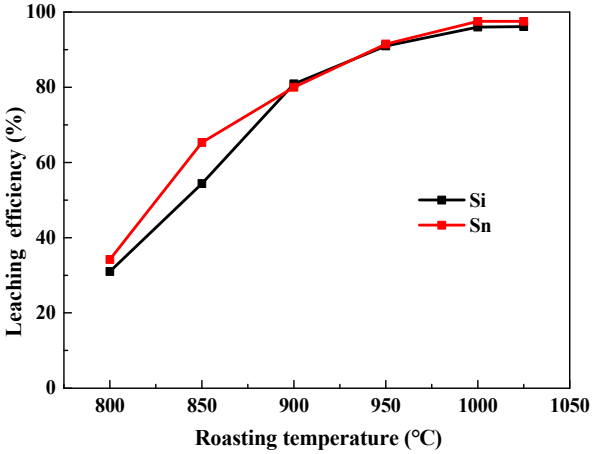

Figure 1. Effect of roasting temperature on leaching efficiency of Sn and Si (Time: 60 min).

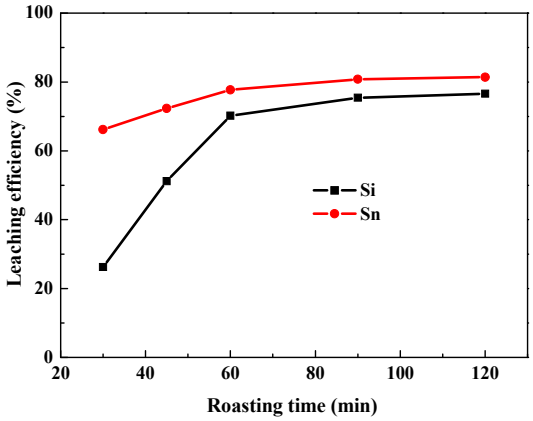

Figure 2. Effect of roasting time on leaching efficiency of Sn and Si (Temperature: 875 °C).

Figure 2 shows the effect of roasting time in the range of 30–120 min on the leaching efficiency of Sn and Si. The leaching efficiency of Si increased from 26.3 wt. % to 70.2 wt. % as the roasting time increased from 30 to 60 min, while the Sn leaching efficiency was higher than 65 wt. % as the roasting time prolonged. The results indicated that reaction rate of Equation (2) was much faster than that of Equation (3) in CO–CO_2 atmosphere.

$$SnO_2 + Na_2CO_3 = Na_2SnO_3 + CO_2 \quad (2)$$

$$SiO_2 + Na_2CO_3 = Na_2SiO_3 + CO_2 \quad (3)$$

When the roasting time was further extended to 90 min, the leaching efficiency of Sn and Si almost stayed unchanged. As the roasting time was 120 min, the leaching efficiency of Sn and Si was 81.4 wt. % and 76.6 wt. %, respectively.

Based on the results given in Figures 1 and 2, the distribution of Sn and Si elements in the whole experimental flowsheet is presented in Figure 3. The content of Sn and Si in pretreated cassiterite concentrates were 62.9 wt. % and 3.7 wt. %, respectively. Then, the roasted samples were leached in the setting experimental conditions. 70.2 wt. % of Si entered the leachate. Meanwhile, it was worthy to note that leaching efficiency of Sn was 77.7 wt. % and 22.3 wt. % Sn entered the residues. To discover the underlying reason, the phase components of roasted samples and leach residues should be further determined.

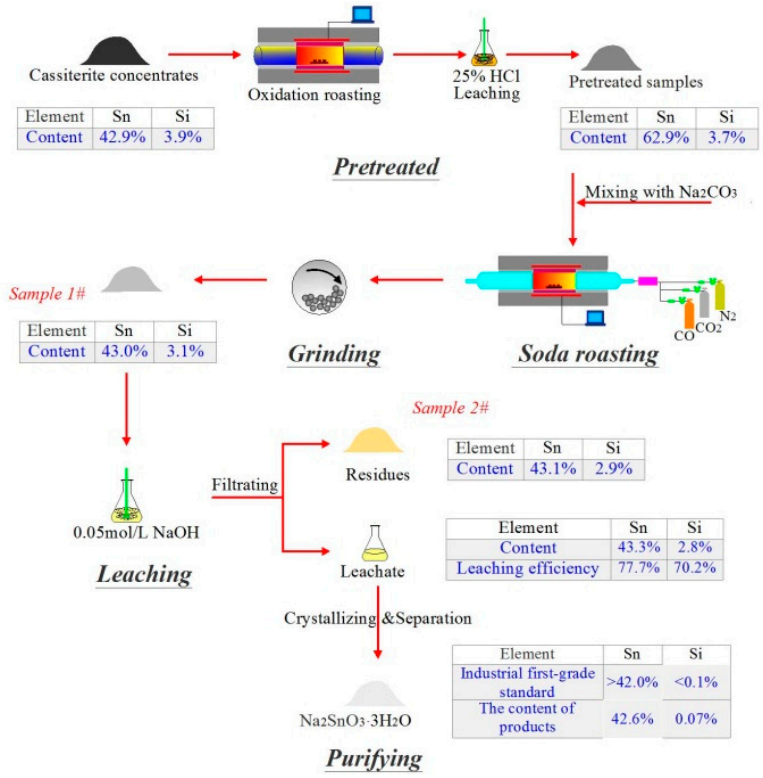

Figure 3. Distribution of Sn and Si elements in the whole experimental flowsheet (under the most suitable conditions).

3.1.2. Phase Analysis of Roasted Samples and Leach Residues

The XRD pattern raw material (in Figure 3) is shown in Figure 4, which contained tin oxide (SnO_2) and silicon dioxide (SiO_2). The XRD pattern of Sample 1# (in Figure 3) is shown in Figure 5. The main phases of the roasted samples were Na_2SnO_3 and Na_2SiO_3, and the content of Sn and Si was 43.0 wt. % and 3.1 wt. %, respectively (as shown in Figure 3). In particular, the characteristic peaks of $Na_8SnSi_6O_{18}$ were also observed in Figure 5. It was noteworthy that the phase of $Na_8SnSi_6O_{18}$ was never reported in previous researches.

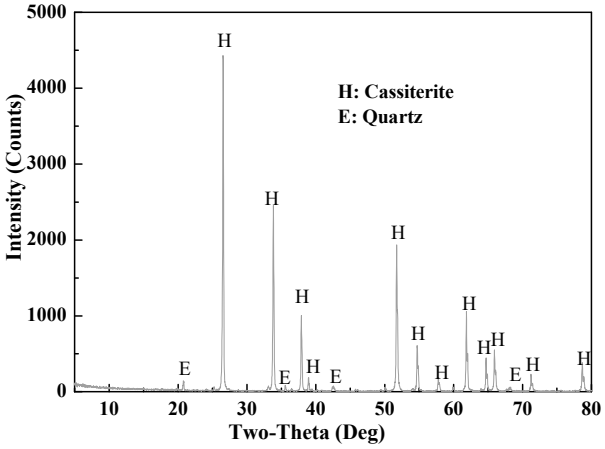

Figure 4. X-ray diffraction pattern of raw material.

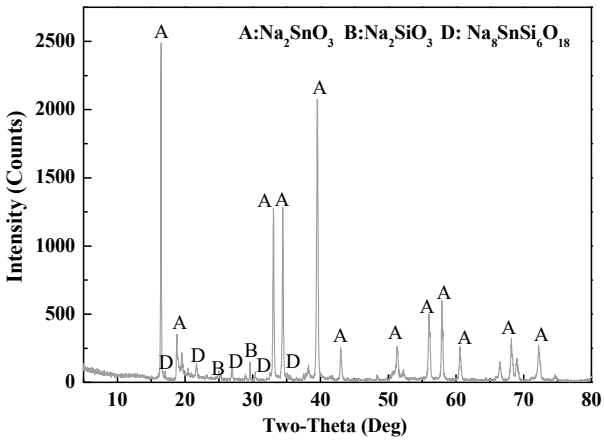

Figure 5. XRD pattern of the roasted samples (Sample 1# in Figure 3).

Sample 1# was then used for the leaching test. The XRD pattern of the leach residues, Sample 2# (in Figure 4), is shown in Figure 6. The content of Sn and Si in the residues was 43.1 wt. % and 2.9 wt. %, as shown in Figure 4. The main phases of the residues were SnO_2 and $Na_8SnSi_6O_{18}$. Moreover, the diffraction intensities of $Na_8SnSi_6O_{18}$ were more intensive compared with those shown in Figure 6, indicating that $Na_8SnSi_6O_{18}$ was enriched in the residues. Meanwhile, the diffraction peaks of Na_2SnO_3 and Na_2SiO_3 disappeared. Therefore, we drew the following conclusions: (1) a few of SnO_2 was were not converted into soluble stannate; (2) $Na_8SnSi_6O_{18}$ was formed in the roasting process; (3) Na_2SnO_3 and Na_2SiO_3 were almost dissolved into the leachate during the leaching process; (4) $Na_8SnSi_6O_{18}$ was possibly insoluble and enriched in the residues.

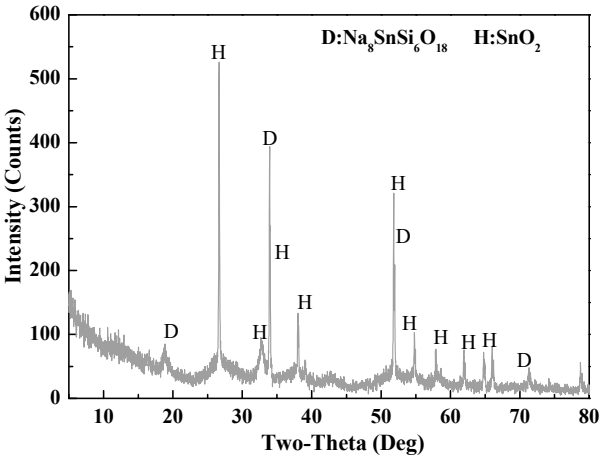

Figure 6. XRD pattern of the leach residues (Sample 2# in Figure 3).

3.1.3. Solution Chemistry of Metasilicic Acid and Tin

To further determine the existing forms of Sn and Si ions in the leachate, the solution chemistry of leachate with different pH value was analyzed. Dissolution thermodynamics of Sn and Si ions in aqueous solution was firstly discussed in the leaching process. In previous publications [35–37], it was reported that Sn(IV) might exist as Sn^{4+}, $SnOH^{3+}$, $Sn(OH)_2^{2+}$, $Sn(OH)_3^{+}$, $Sn(OH)_4$, $Sn(OH)_5^{-}$, and $Sn(OH)_6^{2-}$, while Si(IV) could exist as H_2SiO_3, $HSiO_3^{-}$, and SiO_3^{2-}. The mole fractions of metasilicic and stannum species at varying pH values were calculated based on previous studies (reaction constant (K) shown in Table 2) [38–41], and the results are shown in Figure 7.

Table 2. Reaction constants for equilibrium reactions of Si(IV) and Sn(IV) species.

Equation	Reaction Equation	Equilibrium Constants (*K*)
(4)	$Sn^{4+} + H_2O = Sn(OH)^{3+} + H^+$	$K_{\alpha 1} = 10^{3.73}$
(5)	$Sn^{4+} + 2H_2O = Sn(OH)_2^{2+} + 2H^+$	$K_{\alpha 1} = 10^{1.29}$
(6)	$Sn^{4+} + 3H_2O = Sn(OH)_3^{+} + 3H^+$	$K_{\alpha 1} = 10^{0.47}$
(7)	$Sn^{4+} + 4H_2O = Sn(OH)_4 + 4H^+$	$K_{\alpha 1} = 10^{0.4}$
(8)	$Sn^{4+} + 5H_2O = Sn(OH)_5^{-} + 5H^+$	$K_{\alpha 2} = 10^{-7.7}$
(9)	$Sn^{4+} + 6H_2O = Sn(OH)_6^{2-} + 6H^+$	$K_{\alpha 3} = 10^{-18.1}$
(10)	$SiO_3^{2-} + H+ = HSiO_3^{-}$	$K_{\beta 1} = 10^{-11.82}$
(11)	$HSiO_3^{-} + H+ = H_2SiO_3$	$K_{\beta 2} = 10^{-9.69}$

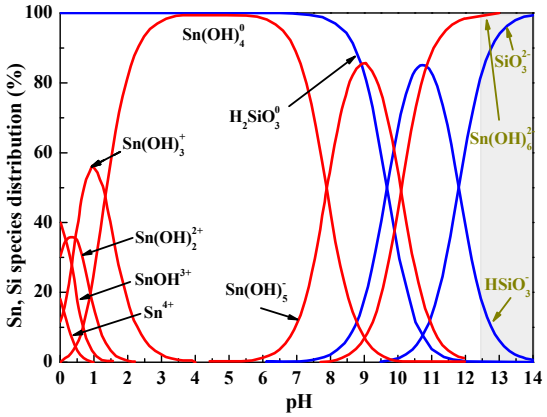

Figure 7. Mole fractions of metasilicic and stannum species at different pH values.

Figure 7 illustrated the very strong hydrolysis behaviors of Si(IV) and Sn(IV). The main species of metasilicic and stannum were Sn^{4+}, $SnOH^{3+}$, $Sn(OH)_2^{2+}$, and H_2SiO_3 at pH value below 2. The neutral $Sn(OH)_4$ and H_2SiO_3 were dominant at pH value of 2–7.5. At pH of 9.5, the negatively charged $HSiO_3^-$, SiO_3^{2-}, $Sn(OH)_5^-$, and $Sn(OH)_6^{2-}$ were the main aqueous species. However, after pH value above 12.5, the mole fraction of $HSiO_3^-$ was lower compared to that of SiO_3^{2-}. Moreover, $Sn(OH)_4$ and H_2SiO_3 disappeared. Generally, a leaching solvent with a pH greater than 12 is preferred for the prevention of stannate hydrolysis [14]. Hence, $Sn(OH)_6^{2-}$ and SiO_3^{2-} only existed in the solution when the value of pH was more than 12.6 (0.05 mol/L NaOH). Figure 6 also indicated that there were no H_2SiO_3(s) and $Sn(OH)_4$(s) in the leach residues, illustrating that H_2SiO_3(s) and $Sn(OH)_4$(s) was not formed during the leaching process.

The possible reaction of Na_2SnO_3(s) during the leaching process was expressed as Equation (12), and $Sn(OH)_6^{2-}$ anions were instantly formed because of their high stability under weakly alkaline condition [42]. Na_2SiO_3(s) was dissolved as forms of Na^+ and SiO_3^{2-} (aq.) by Equation (13) at pH of 12.6 [36]. However, $Sn(OH)_6^{2-}$ did not react with SiO_3^{2-} to form $Na_8SnSi_6O_{18}$ in the solution with pH value of 12.6. Therefore, we inferred that $Na_8SnSi_6O_{18}$ was only formed in the roasting process.

$$Na_2SnO_3(s) + 3H_2O = Na_2Sn(OH)_6\ (aq.) = 2Na^+ + Sn(OH)_6^{2-} \quad (12)$$

$$Na_2SiO_3(s) = 2Na^+ + SiO_3(aq)^{2-} \quad (13)$$

The abovementioned results indicated that SiO_2 in the cassiterite concentrates could react with Na_2CO_3 and SnO_2 to form Na_2SnO_3, Na_2SiO_3, and $Na_8SnSi_6O_{18}$ during the roasting process. Part of SiO_2 reacted with SnO_2 and Na_2CO_3 to form $Na_8SnSi_6O_{18}$. Moreover, Na_2SnO_3 and Na_2SiO_3 were more easily soluble than $Na_8SnSi_6O_{18}$. In order to make sure how $Na_8SnSi_6O_{18}$ was formed during the roasting process, effect of SiO_2 on phase evolution of SnO_2–Na_2CO_3 system was further researched.

3.2. Effect of SiO_2 on Phase Evolution of SnO_2–Na_2CO_3 System

It was reported that SiO_2/SnO_2 molar ratio in cassiterite concentrates was about 1:4 [14]. Hence, in order to research the effect of SiO_2 on phase evolution of SnO_2–Na_2CO_3 system, the analytical grade reagents of Na_2CO_3 and SiO_2 were added into cassiterite concentrates with different SiO_2/SnO_2 molar ratios. In particular, $Na_2CO_3/(SnO_2 + SiO_2)$ mole ratio was fixed as 1.5.

3.2.1. Effect of SiO_2/SnO_2 Mole Ratio

Firstly, different SiO_2 dosage was added into cassiterite concentrates in order to investigate the effect of SiO_2/SnO_2 mole ratio. The XRD patterns of the samples roasted at 875 °C for 60 min in a 15 vol. % CO atmosphere are shown in Figure 8. SiO_2/SnO_2 mole ratio varied in the range of 1:4–7:1.

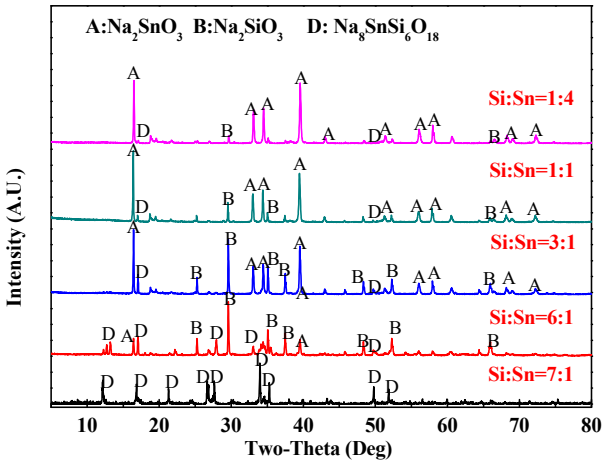

Figure 8. XRD patterns of the samples with different SiO_2/SnO_2 mole ratio (Temperature: 875 °C; Time: 60 min).

As observed from Figure 8, the main phases of the roasted samples were Na_2SnO_3, Na_2SiO_3, and a small amount of $Na_8SnSi_6O_{18}$ when the SiO_2/SnO_2 mole ratio was 1:4. As the SiO_2/SnO_2 mole ratio increased from 1:4 to 7:1, the diffraction peak intensity of $Na_8SnSi_6O_{18}$ increased significantly. Meanwhile, the diffraction peak of Na_2SnO_3 was gradually weakened and vanished. The Sn/Si theoretical value in $Na_8SnSi_6O_{18}$ was 1:6. The results indicated that high Si content in cassiterite concentrates promoted the formation of $Na_8SnSi_6O_{18}$, which decreased the conversion of SnO_2 to Na_2SnO_3 during the roasting process.

3.2.2. Effect of Roasting Temperature

The effect of roasting temperature was then performed, and Figure 9 shows the XRD patterns of the samples roasted for 60 min at temperature range of 775–925 °C. SiO_2/SnO_2 mole ratio was fixed as 7:1.

It was found that the phases of the samples roasted at 775 °C were $Na_8SnSi_6O_{18}$, Na_2SiO_3, and a small amount of Na_2CO_3. The diffraction peak intensities of $Na_8SnSi_6O_{18}$ were enhanced with increasing the roasting temperature, while those of Na_2SiO_3 and Na_2CO_3 were weakened. When the temperature reached at 875 °C, $Na_8SnSi_6O_{18}$ was the predominant substance in the roasted samples. The diffraction peaks of Na_2SiO_3 and Na_2CO_3 almost vanished as the roasting temperature increased to 925 °C, and $Na_8SnSi_6O_{18}$ was the only phase in the roasted samples.

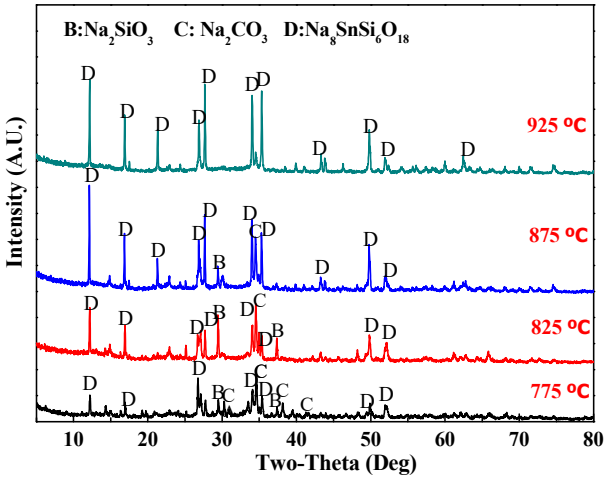

Figure 9. XRD patterns of the samples roasted at different temperatures (Time: 60 min; SiO_2/SnO_2 molar ratio: 7:1).

It was worthy to note that 875 °C was the suitable roasting temperature for Na_2SnO_3 preparation by the soda roasting–leaching process [14]. Besides, as observed from Figure 4, the leaching efficiency of Sn and Si at 875 °C was 77.7 wt. % and 70.2 wt. %, respectively. Furthermore, the leaching efficiency of Sn and Si was derived from the formation of soluble Na_2SnO_3 and Na_2SiO_3. The results further illustrated that a part of SnO_2 and SiO_2 was transformed into $Na_8SnSi_6O_{18}$. The corresponding reaction was expressed as the reaction of Equation (14).

$$SnO_2 + 6SiO_2 + 4Na_2CO_3 = Na_8SnSi_6O_{18} + 4CO_2 \quad (14)$$

3.3. Leaching Behavior of $Na_8SnSi_6O_{18}$

$Na_8SnSi_6O_{18}$ was inevitably formed in the roasting process, and it was enriched in the leach residues. However, the leaching behavior of $Na_8SnSi_6O_{18}$ was never conducted. In this section, to determine the leaching behavior of $Na_8SnSi_6O_{18}$, $Na_8SnSi_6O_{18}$ was synthesized under the following conditions: mole ratio of Na_2CO_3:SnO_2:SiO_2 = 4:1:6, roasting temperature of 1000 °C, and roasting time of 120 min. The XRD pattern of synthetic $Na_8SnSi_6O_{18}$ is shown in Figure 10. The results indicated that the roasted product had a very high purity and was well-matched with the PDF standard card (PDF#72-2449) of $Na_8SnSi_6O_{18}$ phase, and there were no diffraction peaks of other impurities.

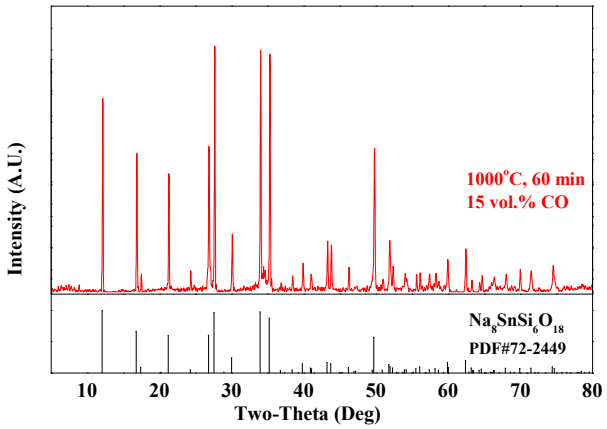

Figure 10. XRD pattern of the synthetic $Na_8SnSi_6O_{18}$.

Effect of pH on leaching behavior of $Na_8SnSi_6O_{18}$ was performed under the following leaching experimental conditions: liquid-to-solid ratio of 4 cm^3/g, leaching temperature of 40 °C, leaching time of 60 min, and stirring rate of 300 rpm [14].

The effect of pH value on the leaching efficiency of Si and Sn was investigated systematically, and the results are shown in Figure 11a. The leaching efficiency of Sn decreased from 65.1 wt. % to 1.9 wt. % and Si from 21.2 wt. % to 4.9 wt. % as the pH value increased from −0.6 (4 mol/L HCl) to 1. The leaching efficiency of Si and Sn was substantially unchanged as the pH value increased further. The leaching efficiency of Sn and Si was 0.5 wt. % and 1.3 wt. % (in Figure 11a) when the pH value was 12.6 (0.05 mol/L NaOH). The XRD pattern of the leach residues obtained at pH of 12.6 is also presented in Figure 11b. It is seen from Figure 11b that $Na_8SnSi_6O_{18}$ was the only phase in the residues. The results verified that $Na_8SnSi_6O_{18}$ phase was almost insoluble and residual in the residues.

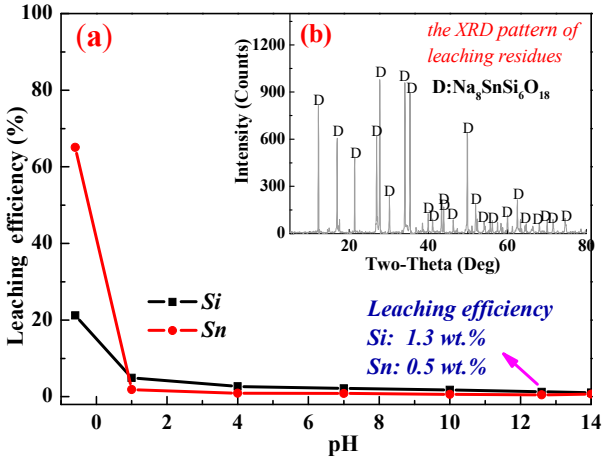

Figure 11. The leaching efficiency Si and Sn of the synthetic $Na_8SnSi_6O_{18}$. (**a**) leaching efficiency Si and Sn, (**b**) XRD pattern of leach residues.

In the whole, $Na_8SnSi_6O_{18}$ was inevitably formed in the roasting process for preparation of Na_2SnO_3 if using cassiterite as raw materials. Moreover, $Na_8SnSi_6O_{18}$ was insoluble in the pH range of 1–14, which was the main reason that part of tin oxides was not converted into soluble Na_2SnO_3 and enriched in the residues. Thus, if cassiterite concentrates were used as raw materials to prepare Na_2SnO_3 by the soda roasting–leaching process, the silicon content in the cassiterite should be controlled as low as possible.

4. Conclusions

In this study, the effect of SiO_2 on sodium stannate preparation from cassiterite and Na_2CO_3 roasted under CO–CO_2 atmosphere was investigated. The main conclusions were summarized as follows:

1. Na_2SnO_3, Na_2SiO_3, and $Na_8SnSi_6O_{18}$ were easily formed when the Na_2CO_3 + SnO_2 + SiO_2 mixtures were roasted under CO–CO_2 atmosphere. Na_2SnO_3 and Na_2SiO_3 were easily dissolved into the leachate during the leaching process, while $Na_8SnSi_6O_{18}$ enriched into the leach residues.
2. $Na_8SnSi_6O_{18}$ was inevitably formed in the roasting process of preparation of Na_2SnO_3. Roasting temperature and Si/Sn mole ratio were the two critical factors affecting the formation of $Na_8SnSi_6O_{18}$, which was more easily formed at higher roasting temperature and Si/Sn mole ratio.
3. The leaching behavior of synthetic $Na_8SnSi_6O_{18}$ indicated that $Na_8SnSi_6O_{18}$ was almost insoluble in the leachate at the pH range of 1–14. Therefore, the loss of tin in the residues was mainly attributed to the insoluble $Na_8SnSi_6O_{18}$ formed during the roasting process.

Author Contributions: Y.Z. conceived the project and wrote the final paper. Z.S. performed the experiments and wrote initial drafts of the work. B.H. performed the experiment. X.C. performed the XRD analysis. M.L., S.L., J.L., and T.J. discussed the content. All authors discussed the results and reviewed the manuscript.

Funding: This research was funded by National Natural Science Foundation of China (No.51574283 and No.51234008).

Acknowledgments: The authors would express their heartful thanks to Financial supports from the National Natural Science Foundation of China and Co-Innovation Center for Clean and Efficient Utilization of Strategic Metal Mineral Resources, and language editing assistance from Corby Anderson in Kroll Institute for Extractive Metallurgy, Colorado School of Mines, USA.

Conflicts of Interest: The authors declare no conflict of interest.

References

1. Sharma, A.; Das, S.; Das, K. Effect of different electrolytes on the microstructure, corrosion and whisker growth of pulse plated tin coatings. *Microelectron. Eng.* **2017**, *170*, 59–68. [CrossRef]
2. Yang, W.; Xu, D.; Yao, X. Stable preparation and characterization of yellow micro arc oxidation coating on magnesium alloy. *J. Alloy. Compd.* **2018**, *745*, 609–616. [CrossRef]
3. Zhang, S.G.; Wei, Y.D.; Yin, S.F.; Luo, S.L.; Au, C.T. Superbasic sodium stannate as catalyst for dehydrogenation, Michael addition and transesterification reactions. *Appl. Catal. A Gen.* **2011**, *406*, 113–118. [CrossRef]
4. Sang, B.; Li, Z.; Yu, L.; Li, X.; Zhang, Z. Preparation of zinc hydroxystannate-titanate nanotube flame retardant and evaluation its smoke suppression efficiency for flexible polyvinyl chloride matrix. *Mater. Lett.* **2017**, *204*, 133–137. [CrossRef]
5. Butova, V.V.; Shukaev, I.L. Ion exchange conversion of solid electrolyte, potassium sodiostannate, into isomorphous metastable sodium stannate. *Mendeleev Commun.* **2016**, *26*, 246–247. [CrossRef]
6. Wang, L.; Pu, S. Direct preparation of sodium stannate from tin concentrates. *J. Cent. South Inst. Min. Metall.* **1987**, *18*, 427–431.
7. Liu, W.; Li, W.; Han, J.; Wu, D.; Li, Z.; Gu, K.; Qin, W. Preparation of calcium stannate from lead refining slag by alkaline leaching-purification-causticization process. *Sep. Purif. Technol.* **2019**, *212*, 119–125. [CrossRef]
8. Wu, D.; Liu, W.; Han, J.; Jiao, F.; Xu, J.; Gu, K.; Qin, W. Direct preparation of sodium stannate from lead refining dross after NaOH roasting-water leaching. *Sep. Purif. Technol.* **2019**, *227*, 115683. [CrossRef]
9. Liu, W.; Li, Z.; Han, J.; Li, W.; Wang, X.; Wang, N.; Qin, W. Selective Separation of Arsenic from Lead Smelter Flue Dust by Alkaline Pressure Oxidative Leaching. *Minerals* **2019**, *9*, 308. [CrossRef]
10. Wu, D.; Han, J.; Liu, W.; Jiao, F.; Qin, W. Preparation of Calcium Stannate from Lead Refining Dross by Roast–Leach–Precipitation Process. *Minerals* **2019**, *9*, 283. [CrossRef]
11. Akimoto, Y.; Iizuka, A.; Shibata, E. High-voltage pulse crushing and physical separation of polycrystalline silicon photovoltaic panels. *Miner. Eng.* **2018**, *125*, 1–9. [CrossRef]
12. Yang, C.; Li, J.; Tan, Q.; Liu, L.; Dong, Q. Green process of metal recycling: Coprocessing waste printed circuit boards and spent tin stripping solution. *ACS Sustain. Chem. Eng.* **2017**, *5*, 3524–3534. [CrossRef]
13. Yang, C.; Tan, Q.; Liu, L.; Dong, Q.; Li, J. Recycling Tin from electronic waste: A problem that needs more attention. *ACS Sustain. Chem. Eng.* **2017**, *5*, 9586–9598. [CrossRef]
14. Zhang, Y.; Su, Z.; Liu, B.; You, Z.; Yang, G.; Li, G.; Jiang, T. Sodium stannate preparation from stannic oxide by a novel soda roasting–leaching process. *Hydrometallurgy* **2014**, *146*, 82–88. [CrossRef]
15. Liu, B.; Zhang, Y.; Su, Z.; Li, G.; Jiang, T. Phase Evolution of Tin Oxides Roasted Under CO–CO_2 Atmospheres in the Presence of Na_2CO_3. *Miner. Process. Extr. Metall. Rev.* **2016**, *37*, 264–273. [CrossRef]
16. Liu, B.; Zhang, Y.; Su, Z.; Li, G.; Jiang, T. Function mechanism of CO-CO_2 atmosphere on the formation of Na_2SnO_3 from SnO_2 and Na_2CO_3 during the roasting process. *Powder Technol.* **2016**, *301*, 102–109. [CrossRef]
17. Su, Z.; Zhang, Y.; Liu, B.; Chen, J.; Li, G.; Jiang, T. Effect of $CaCO_3$ on the Gaseous Reduction of Tin Oxide Under CO-CO_2 Atmosphere. *Miner. Process. Extr. Metall. Rev.* **2016**, *37*, 179–186. [CrossRef]
18. Su, Z.; Zhang, Y.; Liu, B.; Chen, Y.; Li, G.; Jiang, T. Effect of CaF_2 On the Reduction Volatilization of Tin Oxide Under CO-CO_2 Atmosphere. *Miner. Process. Extr. Metall. Rev.* **2017**, *38*, 207–213. [CrossRef]

19. Liu, B.; Zhang, Y.; Su, Z.; Li, G.; Jiang, T. Formation kinetics of Na_2SnO_3 from SnO_2 and Na_2CO_3 roasted under CO-CO_2 atmosphere. *Int. J. Miner. Process.* **2017**, *165*, 34–40. [CrossRef]
20. Zhang, Y.; Su, Z.; You, Z.; Liu, B.; Yang, G.; Li, G.; Jiang, T. Sodium stannate preparation from cassiterite concentrate and sodium carbonate by roasting under a CO–CO_2 atmosphere. In Proceedings of the Rare Metal Technology, Conference Proceeding, TMS, San Diego, CA, USA, 16–20 February 2014; pp. 163–169.
21. Feng, Q.; Wen, S.; Zhao, W.; Chen, Y. Effect of calcium ions on adsorption of sodium oleate onto cassiterite and quartz surfaces and implications for their flotation separation. *Sep. Purif. Technol.* **2018**, *200*, 300–306. [CrossRef]
22. Tian, M.; Zhang, C.; Han, H.; Liu, R.; Gao, Z.; Chen, P.; He, J.; Hu, Y.; Sun, W.; Yuan, D. Novel insights into adsorption mechanism of benzohydroxamic acid on lead (II)-activated cassiterite surface: An integrated experimental and computational study. *Miner. Eng.* **2018**, *122*, 327–338. [CrossRef]
23. Wright, P.A. *Extractive Metallurgy of Tin*, 2nd ed.; Elsevier: Amsterdam, The Netherlands, 1982.
24. Song, X.C. *Tin Metallurgy*; Metallurgical Industry Press: Beijing, China, 2011.
25. Paparoni, G.; Webster, J.D.; Walker, D. Experimental techniques for determining tin solubility in silicate melts using silica capsules in 1 atm furnaces and rhenium capsules in thepiston cylinder. *Am. Mineral.* **2010**, *95*, 776–783. [CrossRef]
26. Zhang, Y.; Su, Z.; Liu, B.; Zhou, Y.; Jiang, T.; Li, G. Reduction behavior of SnO_2 in the tin-bearing iron concentrates under CO-CO_2 atmosphere. Part II: Effect of quartz. *Powder Technol.* **2016**, *291*, 337–343. [CrossRef]
27. Zhang, Y.; Liu, B.; Su, Z.; Chen, J.; Li, G.; Jiang, T. Effect of Na_2CO_3 on the preparation of metallic tin from cassiterite roasted under strong reductive atmosphere. *J. Min. Metall.* **2016**, *52*, 9–15. [CrossRef]
28. Sanchez-Segado, S.; Monti, T.; Katrib, J.; Kingman, S.; Dodds, C.; Jha, A. Towards sustainable processing of columbite group minerals: Elucidating the relation between dielectric properties and physico-chemical transformations in the mineral phase. *Sci. Rep.* **2017**, *7*, 18016. [CrossRef]
29. Escudero-Castejon, L.; Sanchez-Segado, S.; Parirenyatwa, S.; Hara, Y.; Jha, A. A Cr^{6+}-free extraction of chromium oxide from chromite ores using carbothermic reduction in the presence of alkali. In *Applications of Process Engineering Principles in Materials Processing, Energy and Environmental Technologies*; Springer: Berlin/Heidelberg, Germany, 2017; pp. 179–188.
30. Parirenyatwa, S.; Escudero-Castejon, L.; Sanchez-Segado, S.; Hara, Y.; Jha, A. An investigation on the kinetics and mechanism of alkali reduction of mine waste containing titaniferous minerals for the recovery of metals. In *Applications of Process Engineering Principles in Materials Processing, Energy and Environmental Technologies*; Springer: Berlin/Heidelberg, Germany, 2017; pp. 465–474.
31. Sanchez-Segado, S.; Lahiri, A.; Jha, A. Alkali roasting of bomar ilmenite: Rare earths recovery and physico-chemical changes. *Open Chem.* **2015**, *13*, 270–278. [CrossRef]
32. Su, Z.; Zhang, Y.; Han, B.; Liu, B.; Lu, M.; Peng, Z.; Li, G.; Jiang, T. Synthesis, characterization, and catalytic properties of nano-SnO by chemical vapor transport (CVT) process under CO–CO_2 atmosphere. *Mater. Des.* **2017**, *121*, 280–287. [CrossRef]
33. Knutsson, P.; Lai, H.; Stiller, K. A method for investigation of hot corrosion by gaseous Na_2SO_4. *Corros. Sci.* **2013**, *73*, 230–236. [CrossRef]
34. Li, Y.; He, J.B.; Zhang, M.; He, X.L. Corrosion inhibition effect of sodium phytate on brass in NaOH media. Potential-resolved formation of soluble corrosion products. *Corros. Sci.* **2013**, *74*, 116–122. [CrossRef]
35. Séby, F.; Potin-Gautier, M.; Giffaut, E.; Donard, O.F.X. A critical review of thermodynamic data for inorganic tin species. *Geochim. Cosmochim. Acta* **2001**, *65*, 3041–3053. [CrossRef]
36. Park, H.; Englezos, P. Osmotic coefficient data for Na_2SiO_3 and Na_2SiO_3-NaOH by an isopiestic method and modeling using Pitzer's model. *Fluid Phase Equilib.* **1998**, *153*, 87–104. [CrossRef]
37. Kim, E.; Osseo-Asare, K. Dissolution windows for hydrometallurgical purification of metallurgical-grade silicon to solar-grade silicon: Eh-pH diagrams for Fe silicides. *Hydrometallurgy* **2012**, *127*, 178–186. [CrossRef]
38. Zhao, Z.; Shuai, W.; Zhang, J.; Chen, X. Sn (IV) anions adsorption onto ferric hydroxide: A speciation-based model. *Hydrometallurgy* **2013**, *140*, 135–143. [CrossRef]
39. Lindsay, W.L. *Chemical Equilibria in Soils*; Wiley: New York, NY, USA, 1979; pp. 79–85.
40. Hummel, W.; Berner, U.; Curti, E.; Pearson, F.J.; Thoenen, T. Nagra/PSI chemical thermodynamic data base 01/01. *Radiochim. Acta* **2002**, *90*, 805–813. [CrossRef]

41. Angadi, S.I.; Sreenivas, T.; Jeon, H.S.; Baek, S.H.; Mishra, B.K. A review of cassiterite beneficiation fundamentals and plant practices. *Miner. Eng.* **2015**, *70*, 178–200. [CrossRef]
42. Choi, Y.I.; Salman, S.; Kuroda, K.; Okido, M. Synergistic corrosion protection for AZ31 Mg alloy by anodizing and stannate post-sealing treatments. *Electrochim. Acta* **2013**, *97*, 313–319. [CrossRef]